

PHY 445/515: Phase Transitions

Max Podgorski and Chase Wallace
Stony Brook University
(Dated: May 14, 2021)

In this report, the first order metal-insulator phase transition in vanadium dioxide (VO_2) and the second order phase paraelectric-ferroelectric transition in Barium titanate (BaTiO_3) are investigated. In VO_2 we measured the critical temperature to be $T_c = 65.0 \pm 0.4 \text{ }^\circ\text{C}$ with a coercive temperature of $T^* = 3.7 \pm 0.4 \text{ }^\circ\text{C}$, the semiconducting gap E_g was found to be $0.027 \pm 0.003 \text{ eV}$. The percolation temperatures T_M , absolute resistivities ρ , and the ratio of resistances between the semiconducting and metallic states were also measured. For BaTiO_3 , we found the critical temperature to be $T_c = 126.5 \pm 4 \text{ }^\circ\text{C}$ and the Curie-Weiss constant for $T > T_c$ to be $C_{CW} = (3.9 \pm 0.4) \times 10^4 \text{ K}$. From this value the microscopic dipole moment p and the effective atomic displacement x that is responsible for p were found. We also were able to determine the relative dielectric constant k between the temperatures of $70 \text{ }^\circ\text{C}$ and $150 \text{ }^\circ\text{C}$. Results show the functions and features of first- and second-order phase transitions of these types.

I. INTRODUCTION

The investigation into phase transitions between various states of matter has long been a function of science. For a long time, phase transitions were denoted as such transitions between states of solid, liquid, and gas. Yet modern materials science has shown that all materials have fundamental structural changes as temperature varies. In certain materials, these transitions show both unique and useful changes in measurable qualities. In particular, Vanadium Dioxide, or VO_2 , shows a transition from behaviors of a semiconductor to a metal with an increase in temperature, and Barium Titanite, BaTiO_3 , is Ferroelectric, which has features of varied capacitance at different temperatures.

II. THEORY

A. Phase Transitions

The orders of phase transitions is divided into two levels: first-order transitions are defined by transference of latent heat, whereas a second-order transition is characterised by an order parameter equal to zero as approached from one side of the transition, and some increasing nonzero value on the other. [1]

The Metal-Insulator transition we will investigate in this report is a first-order transition, whereas the ferroelectric transition is one such example of a second-order transition. We will begin by discussing the thermodynamics of the first-order transitions;

B. First Order

From Landau Theory[1], we define the free energy for first-order transitions as

$$F(T, \eta) = A(T)\eta^2 - B_0\eta^4 + C_0\eta^6 \quad (1)$$

The temperature T_0 is that where $A(T)$ changes sign in the function

$$A(T) = A_0(T - T_0) \quad (2)$$

Effectively, what happens from this equation is that there exists a discontinuity in the order parameter as a function of temperature. We also define T^* as

$$T^* = T_0 + \frac{B_0^2}{4A_0C_0} \quad (3)$$

T^* is considered the coercive temperature, which is not the temperature where $A(T)$ goes to zero. Free energy is always continuous, but the first derivative of the free energy at this point is discontinuous, making this a first-order transition.

C. Second Order

In the case of our free energy function being a series expansion

$$F(T, \eta) - F_0 = a(T)\eta^2 + \frac{b(T)}{2}\eta^4 + \dots \quad (4)$$

the solutions to the minimization problem is are

$$\eta = 0 \quad (5)$$

$$\eta_0^2 = -\frac{a}{b} \quad (6)$$

the later of which is augmented as a function of temperature to be

$$\eta_0^2 = -\frac{a_0}{b_0}(T - T_c) \quad (7)$$

From this we can find the value of two parameters, the Free Energy,

$$F - F_0 = \begin{cases} -\frac{a_0^2}{2b_0}(T - T_0)^2, & T < T_c \\ 0, & T > T_c \end{cases} \quad (8)$$

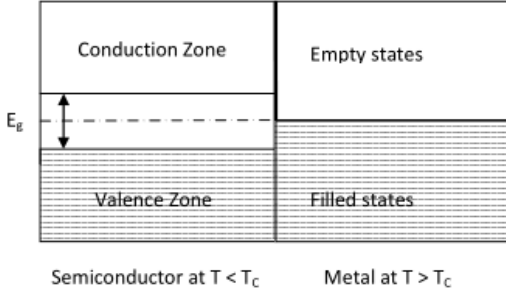


FIG. 1: Visualization of the semiconductor gap in VO₂, [2]

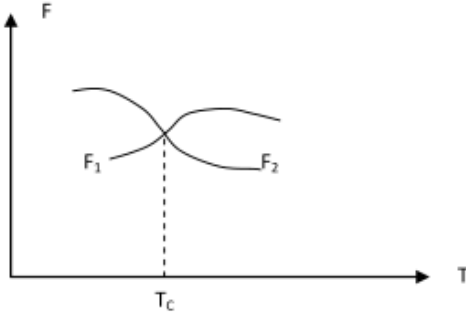


FIG. 2: Visualization of the free energy on both sides of the critical temperature, [2]

and the Specific Heat,

$$c_p = \begin{cases} \frac{a_0^2}{b_0} T, & T < T_c \\ 0, & T > T_c \end{cases} \quad (9)$$

Additionally of note is that in this case the first derivative of the free energy is continuous and it is the second derivative that displays discontinuity.

D. What we expect

When we plot the resistance versus temperature for the Vanadium, we should notice a difference between the energies of the valence and conduction zones. This will appear on our graph as the semiconductor gap existing on one side of the phase transition, but not the other. See Figure 1.

We can also see the differences in the free energy from both sides of the critical temperature, as shown in Figure 2.

The Hysteresis in VO₂ will depend on both the specific sample we are dealing with and with the rate of temperature change that we are conducting our investigations with. Depending on the thickness of our film, the degree of the hysteresis and the change in resistance can vary,

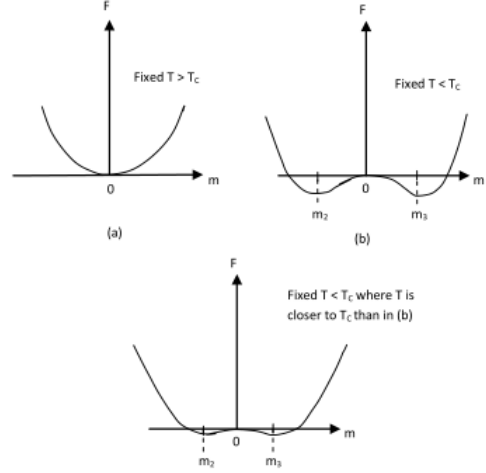


FIG. 3: Graph of the Free Energy for Barium Titanite, showing the double well potential behavior, [2]

but all samples will show the general shape and a critical temperature close to the theoretical value, which would be sufficient to confirm the physical theory.

The energy band gap for materials is defined as

$$E_g = E_g(0) - \frac{\alpha T^2}{T + \beta} \quad (10)$$

Note that Band Gaps vary not only by sample, but by the definition of what the band gap is. Our reference source measures it as the difference between the fermi level and the top of the valence band, so we expect it to be in a range provided in our table below. [3] Additionally, semiconductor resistivity with respect to temperature is defined as

$$\rho = \rho_0 e^{\frac{E_g}{2kT}} \quad (11)$$

which is how we determined the band gap energy [3].

For Barium Titanite, one thing we expect to see is the characteristic double well potentials. Figure 3 shows a graph of the free energy in Barium Titanite at three different temperatures depending on the order parameter, which indicates the fluctuating double wells whose size is dependant on temperature. In particular, Barium Titanite's second-order transition is from a paraelectric to a ferroelectric across a temperature around 120 °C. We're also going to want to find the value of k in the following equation:

$$C = \frac{\epsilon_0 k A}{d} \quad (12)$$

This value may vary depending on the sample, since k the relative dielectric constant, $k = \frac{C}{C_0}$. Near, and above, the phase transition we can use the approximation

$$\chi_E \approx \frac{C_{CW}}{T - T_c} \approx k(T) \quad (13)$$

for T close to T_c and $T > T_c$. From the Curie-Weiss constant C_{CW} , the microscopic dipole moment p can be calculated (see [2] for detail) using

$$p = \sqrt{\frac{\epsilon_0 k_b C_{CW}}{N}} = 6 e^- x \quad (14)$$

where N is

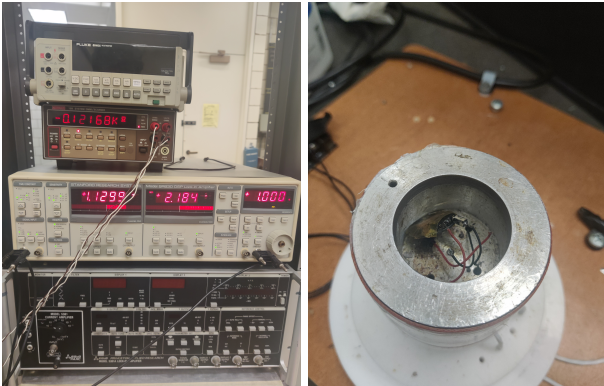
$$N = \frac{1}{a^3} = \frac{1}{65.723 \text{ \AA}^3} = \frac{1}{6.5723 \times 10^{-29} \text{ m}^3} \quad (15)$$

a comes from [4] with negligible uncertainties.

III. MEASUREMENTS

A. Lock-In Amplifiers

Lock-In Amplifiers allow us to remove a lot of signal noise, meaning that we can take meaningful data precisely, even with low currents. It, most importantly for our purposes, allows us to measure signals in and out of phase, which allows the measurements of resistance and capacitance that we need. The amplifier also removes offsets and drifts, which increases the precision of our data. More about Lock-In Amplifiers, the theory behind their operation, and features can be found in [5]. We used a SR830 DSP lock-in amplifier (Fig. 4a) with current modulated at 25kHz with a 1V amplitude.



(a) SR830 DSP Lock-in Amplifier (b) Heating chamber with VO_2 sample loaded

FIG. 4: Experimental Apparatus

B. Samples

Both of our samples were provided to us already made. Measurements of the samples were conducted using calipers. These samples had been tested by other groups already and are likely damaged in various ways.

C. Data Acquisition

The majority of the data is taken automatically for us using the LabVIEW software package. This records temperature of our sample chamber (Fig. 4b) and using the data from the amplifier's in and out of phase voltages, it can calculate the resistance of the circuit. For reference, circuit diagrams are provided in [2]. In the case of Vanadium, measurements are using the in-phase voltage, whereas for barium it is the out-phase voltage. It is important to note that the decade resistor was not working at the start of our experiment and was forgone. The only 'extra' resistance that we were able to use was the internal resistance of the lock-in amplifier which was found from the manual.

By measuring the resistance vs. temperature in VO_2 (Fig. 5), the values in table I were extracted.

Value	Literature	Experimental
T_c [°C]	66.9 [6]	65.0 ± 0.4
T^* [°C]	9.0 [3]	3.7 ± 0.4
SC T_M [°C]	—	45.5 ± 0.5
M T_M [°C]	—	90.0 ± 0.5
SC ρ [$k\Omega \cdot m$]	—	35 ± 18
M ρ [$k\Omega \cdot m$]	—	1.2 ± 0.6
R Ratio (R_{SC}/R_M)	—	35 ± 10
E_g [eV]	0.2 - 0.7 [3]	0.027 ± 0.003

TABLE I: Literature and Experimental values for VO_2 ; SC indicates the semiconducting state and M indicates the metallic state

Similarly, by measuring the capacitance vs. temperature in BaTiO_3 (Fig. 9), the relative dielectric constant vs. temperature (Fig. 10) and the values in table II were extracted.

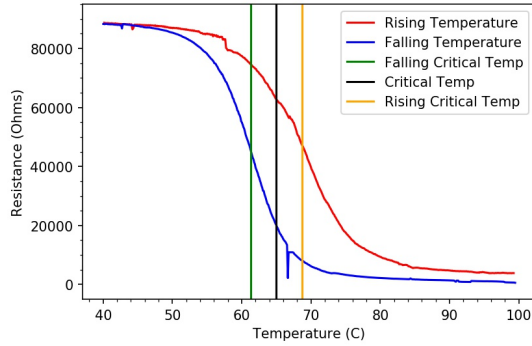
Value	Literature [7]	Experimental
T_c [°C]	125	126.5 ± 4
C_{CW} ($T > T_c$) [K]	1.5×10^5	$(3.9 \pm .4) \times 10^4$
p [$C \cdot m$]	3.5×10^{-29} †	$(2 \pm 0.5) \times 10^{-29}$
x [Å]	0.36 †	$0.18 \pm .05$

TABLE II: Literature and Experimental values for BaTiO_3 ; †calculated from literature C_{CW} value

IV. ANALYSIS

A. VO_2

The resistance of the sample was not directly measured, instead voltage was measured then the resistance of the sample was inferred by the current used, as outlined by equation 16, where I_0 , V_0 , R_0 is the internal current, voltage, and resistance, respectively, of the lock-in amplifier.

FIG. 5: Resistance vs. Temperature in VO_2

$$R = \frac{V_{Mes}}{I_0} = V_{Mes} \frac{R_0}{V_0} = V_{Mes} \frac{1M\Omega}{1V} \quad (16)$$

The data was then split into the rising and falling temperature components for separate analysis. For rough resistance error determination each section was subsequently split into three separate sections, semiconducting, transitioning, and metallic. In each of these sections a small sample was taken, fit with a linear function and the reduced chi squared defined to be 1.

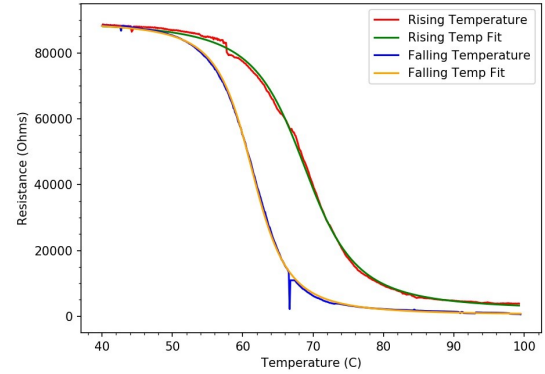
1. T_c, T^*

To find the critical temperatures of the rising and falling temperatures sections, each was fit to a 'guess' function $\propto x/\sqrt{x^2 + 1}$, which has no physical motivation other than expected behavior at low and high temperature values with a central inflection point. This function followed the data well as seen in figure 6, but it was not a good fit to the data as indicated by a large reduced chi squared. However, the inflection point could still be extracted as the critical temperature of that section. This was justified by interpreting the vertical residuals as approximate error and by dividing this error by the slope at that point, the approximate critical temperature values were obtained.

T_c was then determined by the weighted average between the rising and falling T_c values and T^* was determined to be half of the difference between the rising and falling T_c values.

2. $T_M, \rho, (R_{SC}/R_M)$

The percolation temperatures T_M , resistivities ρ , and the resistance ratio R_{SC}/R_M were all determined from data from figure 7. The temperature at which the rising and falling data differed by one standard deviation in the semiconducting region was taken as the semiconducting percolation temperature, the error was then roughly estimated accordingly. The metal percolation temperature

(a) Guess fits for $R(T)$

(b) Fit residuals

FIG. 6: Critical temperature determination for VO_2

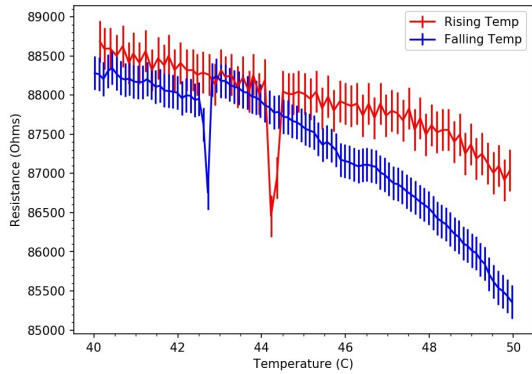
was found in a similar way, however, the resistances in that region were not comparable. To compare the data the rising and falling curves were shifted to their average (in that region) and the process used for the semiconductor temperature was repeated here.

Then the resistances for each phase were taken as the weighted average from the extrema of temperature measurements taken to their respective percolation temperatures. The resistivities were then estimated using equation 17 with errors propagated through. The errors on the resistance ratio were only roughly estimated because of the vast discrepancy in the metal phase resistance values.

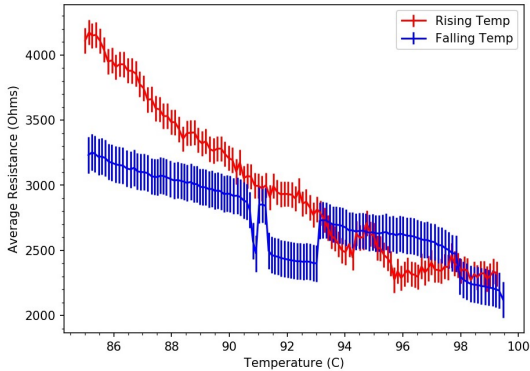
$$\rho = R_{avg} \frac{A}{L} = R_{avg} \frac{\pi r^2}{L} = \pi R_{avg} \frac{(11 \pm 0.5mm)^2}{(1 \pm 0.5mm)} \quad (17)$$

3. E_g

The semiconducting gap was determined by rearranging equation 11 to equation 18, and then plotting and fitting $\ln(R)$ vs. $1/T$ to a linear function, as in figure 8. The slope of the line (multiplied by $2 k_b$ gives us our semiconducting gap directly. A weighted average of the rising and falling temperature values were taken to be the



(a) Semiconducting state



(b) Metallic state

FIG. 7: Determination of percolation temperatures and resistivities for VO_2

true measured value and the error comes directly from the linear fits.

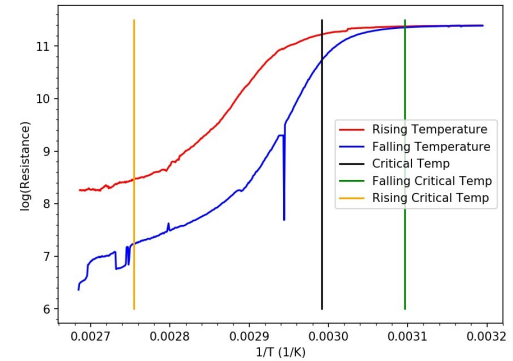
$$\ln(R) = \frac{E_g}{2 k_b} \left(\frac{1}{T} \right) + \ln(R_0) \quad (18)$$

B. BaTiO_3

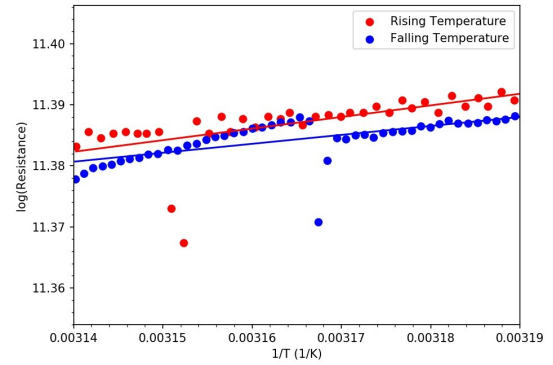
Similar to VO_2 , the capacitance of the sample was not directly measured, instead voltage was measured, then the capacitance of the sample was inferred using equation 19, where f_0 , R_0 is the frequency of the AC oscillation and the internal resistance of the lock-in amplifier, respectively.

$$C = \frac{V_{Mes}}{f_0 R_0} = \frac{V_{Mes}}{(25\text{kHz})(1k\Omega)} \quad (19)$$

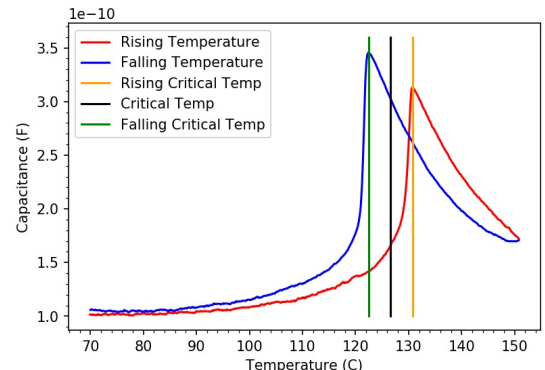
The data was then split into the rising and falling temperature components for separate analysis. The full plot error was determination by taking a small sample from each component, fitting them with a linear function and defining the reduced chi squared to be 1.



(a) All temperatures



(b) Only the semiconducting state

FIG. 8: Determination of the Semiconducting Gap E_g in VO_2 FIG. 9: Capacitance vs. Temperature in BaTiO_3

1. T_c

The temperature at which the capacitance is at a local maximum was taken to be the critical temperature for that component. The errors on each of those values were estimated by looking at the range of temperatures at which the capacitance lied within 1 standard deviation of the maximum capacitance.

The critical temperature reported was the average between the rising and falling critical temperatures, and

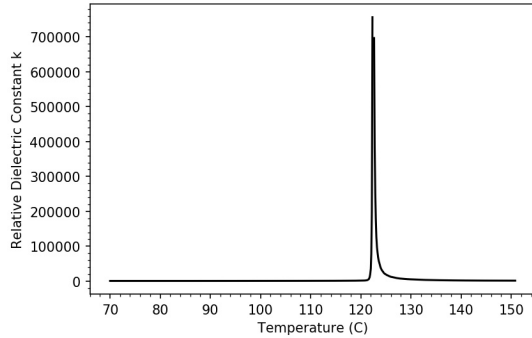


FIG. 10: Relative Dielectric Constant vs. Temperature in BaTiO_3 for the falling temperature measurement

the error was determined to be half of the difference between them. This differs from the VO_2 analysis because BaTiO_3 has a second order phase transition, thus the phase transition should only happen at one temperature.

2. C_{CW} , p , x

To determine the Curie-Weiss constant only the data in the proximity of the critical temperature was considered. Furthermore, the data points immediately surrounding the critical temperature were neglected because Landau theory breaks in the immediate vicinity of the critical temperature and the phase transition has higher order effects.

To measure the Curie-Weiss constant we used the approximation as described in equation 13, which requires us to know the relative dielectric constant $k(T)$.

From our data we can find $k(T)$ as

$$k(T) = \frac{C_{BTO}(T)}{C_0} \approx \frac{C_{mes}(T_c) C_{mes}(T)}{C_0 (C_{mes}(T_c) - C_{mes}(T))} \quad (20)$$

where C_{BTO} is approximated from,

$$C_{mes}(T) \approx \left(\frac{1}{C_{mes}(T_c)} + \frac{1}{C_{BTO}(T)} \right) \quad (21)$$

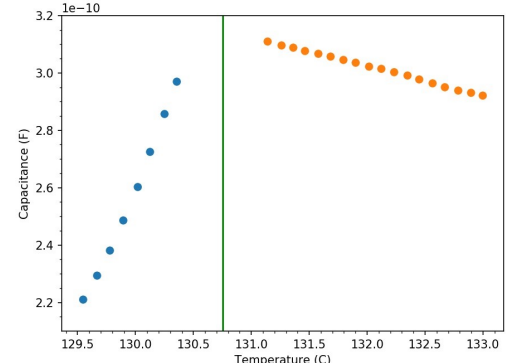
and C_0 is the capacitance of an empty capacitor with the same geometry as our sample,

$$C_0 = \epsilon_0 \frac{A}{d} = \epsilon_0 \frac{(10 \pm 1\text{mm})(8 \pm 1\text{mm})}{(3 \pm 1\text{mm})}$$

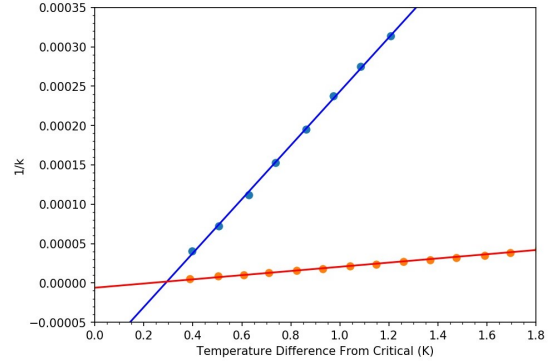
Note, the errors of the measurements used here are larger than that used for VO_2 because the sample has many visible surface imperfections.

So then by plotting and fitting $1/k(T)$ vs. $T - T_c$ to a linear function (Figure 11 b), the slope of the fit for values with $T > T_c$ (Red) is $1/C_{CW}$. The error for C_{CW} was thus determined by propagating the error in this slope.

Using equation 14, the microscopic dipole moment p and effective atomic displacement x were calculated from this found value of C_{CW} .



(a) $C(T)$ with non-second order points removed



(b) Fig. 11a plotted as $1/k$ vs. $T - T_c$

FIG. 11: Determination of the Curie-Weiss Constant in BaTiO_3

V. DISCUSSION

Despite the discrepancies between the literature values reported and our experimentally determined values, we can be fairly confident in our results. Most of these quantities are very sample dependent and require much more precise measurement techniques over greater temperature ranges than what we were capable of. Furthermore, the samples that we used were not synthesized by us and had been used many times over by other lab groups which has likely resulted in damage to the samples.

Another likely cause for the discrepancies was that the temperature of the sample was not directly being measured, rather, inferred from the heating device's electrical data. Evidence for this being a source of systematic error can be seen in the capacitance vs. temperature measurement of BaTiO_3 in Fig. 9. This could explain some of the difference between the two separate critical temperatures measured.

Overall the general shapes of plots were exactly what we expected, the critical temperatures measured are comparable to literature values and our other measured values match close enough to what was expected given the amount of inestimable systematic errors present.

Appendix A: Error Analysis

All error propagation was done using the general error propagation equation for a general function of N measurements $f(x_1, x_1, \dots, x_N)$ with σ_n being the error associated with the measurement x_n . That propagation formula is

$$\sigma_f^2 = \sum_{n=1}^N \left(\frac{\partial f}{\partial x_n} \right)^2 \sigma_n^2 \quad (\text{A1})$$

Additionally, we have two other functions

$$\bar{x} = \sigma_{\bar{x}}^2 \left(\sum_{n=1}^N \frac{x_n}{\sigma_n^2} \right) \quad (\text{A2})$$

$$\sigma_{\bar{x}}^2 = \left(\sum_{n=1}^N \frac{1}{\sigma_n^2} \right)^{-1} \quad (\text{A3})$$

Averaging of values was done using the weighted averaging equation (Eqn. A2) and weighted error averaging

equation (Eqn. A3) with the averaged value, \bar{x} and N calculated or measured values, x_n , with associated errors $\sigma_{\bar{x}}$ and σ_n .

More details and specific calculations can be found in our lab notebook and in the code mentioned in appendix C.

Appendix B: Author Contributions

Primary work on the sections were split such that Max took the majority of the data, as well as wrote the of the Introduction, Theory, Experimental Setup, and Measurements sections. While Chase wrote the Abstract, Analysis, Discussion, and Appendix sections as well as did all of the data and error analysis. The authors then reviewed, revised, and edited each-others sections to prepare for submission.

Appendix C: Data and Code

The CSV files of the data collected, the code used to generate plots, fits, values, and error analysis, as well as our lab notebook can be viewed at <https://github.com/maxpodgorski/Its-just-a-phase-bro>.

-
- [1] L. D. Landau, E. M. Lifshitz, L. P. Pitaevskii, J. B. Sykes, and M. J. Kearsley, *Statistical physics. Part I*, 3rd ed., Statistical physics, Vol. pt. 1 (Elsevier/Butterworth Heinemann, Amsterdam and Boston, 1980).
 - [2] Stony Brook University, *Phase Transitions: Metal-Insulator transition in VO₂ Phase Transitions: Metal-Insulator transition in VO₂ and Ferroelectric Transition in BaTiO₃* (2012).
 - [3] Shin, Suga, Taniguchi, Fujisawa, Kanzaki, Fujimori, Daimon, Ueda, Kosuge, and Kachi, Vacuum-ultraviolet reflectance and photoemission study of the metal-insulator phase transitions in vo₂, v₆o₁₃, and v₂o₃, Physical Review B **41**, 4993 (1990).
 - [4] T. M. Project, Materials data on batio3 by materials project 10.17188/1204413 (2020).
 - [5] P. H. Sydenham and R. Thorn, *Handbook of measuring system design* (Wiley, Chichester, 2005).
 - [6] C. N. Berglund and H. J. Guggenheim, Electronic properties of vo₂ near the semiconductor-metal transition, Physical Review **185**, 1022 (1969).
 - [7] V. V. Mitić, V. Paunović, and L. Kocić, *Dielectric Properties of BaTiO₃ Ceramics and Curie-Weiss and Modified Curie-Weiss Affected by Fractal Morphology*, Vol. 35 (Ceramic Engineering and Science Proceedings Hoboken, New Jersey, 2015).
 - [8] P. Ghosez, J.-P. Michenaud, and X. Gonze, Dynamical atomic charges: The case of abo₃ compounds, Physical Review B **58**, 6224 (1998).
 - [9] Y. Qi, S. Liu, I. Grinberg, and A. M. Rappe, Atomistic description for temperature-driven phase transitions in batio₃, Physical Review B **94**, 10.1103/PhysRevB.94.134308 (2016).